Structure of six-transmembrane cation channels revealed by single-particle analysis from electron microscopic images

Kazuhiro Mio, Toshihiko Ogura and Chikara Sato*

Neuroscience Research Institute and Japan Biological Information Research Center, National Institute of Advanced Industrial Science and Technology (AIST), Umezono 1-1-4, Tsukuba, Ibaraki 305-8568, Japan. E-mail: ti-sato@aist.go.jp

Six-transmembrane (6-TM) cation channels are plasma membrane-integral components of cellular signaling pathways conserved in almost all species, including animals, plants and some kinds of prokaryotes. These channels selectively permeate cations in response to various signals. In excitable and non-excitable mammalian cells, 6-TM cation channels play fundamental roles, including the generation of action potential and its transmission, the regulation of intracellular ion concentrations, and the activation of signaling cascades by humoral or mechanical pathways. Recently, the structures of three different 6-TM-type cation channels have been determined using single-particle analysis from cryo-electron microscopy images: the voltage-sensitive sodium channel, the IP_3 receptor and the TRPC3 channel. The basic structure of the molecules is similar: a bell-like shape comprising a relatively small extracellular (or luminal) domain, a protein-dense transmembrane domain and an expanded cytoplasmic domain. However, in detail, the cytoplasmic architectures are different from one another and are diversely evolved to their specific physiological functions.

Keywords: electron microscopy; ion channel structure; six-transmembrane; single particles.

1. Introduction

Six-transmembrane (6-TM) cation channels are diversely evolved membrane-integral proteins that include voltage-sensitive Na^+, K^+ and Ca^{2+} channels, the TRP superfamily, and the IP_3 receptors. These channels share the same transmembrane topology, of putative 6-TM segments and a pore-forming region. They are speculated to have evolved from the same prototype (Hille, 2001). Tetramer formation is essential for the function as 6-TM cation channels. Several groups of channels have evolved as 24-TM molecules by repeating duplications of 6-TM segments, and form pseudo-tetramers. These channels permeate cations from outside the cell to inside, or from the intra-cellular ion storage (endoplasmic reticulum; ER) to the cytoplasm, in response to various signals. This process initiates various physiological functions, such as cell excitation, voltage-signal transfer, generation of the second messenger in cell signaling, and maintenance of a steady level of intracellular ion concentration. In spite of their physiological importance, however, structural information about these ion channels is quite limited, mainly because of the difficulty in crystallization.

Single-particle analysis is a computer-aided method for determining protein structure using projection images obtained by electron microscopy (EM) (Frank, 2006; Henderson, 2004; van Heel et al., 2000). This technique has great advantages, especially for analyzing fragile membrane-integral proteins including ion channels, transporters and receptors, and for analyzing large complexes that are difficult to crystallize. Because chemical or mechanical treatment can easily be applied to the solubilized proteins, this technique is also useful for the analysis of snapshots during dynamic conformational changes. In cryo-EM, proteins are usually detected as very faint and obscure particles immersed in a noisy background. To improve the signal-to-noise ratio, particle images are classified into groups and averaged to generate characteristic views. The three-dimensional structure can be reconstructed from two-dimensional averages using a posteriori Euler angle assignment or using the tilting method. We have recently determined the structures of the voltage-sensitive sodium channel (Sato et al., 1998, 2001), the type-1 inositol 1,4,5-trisphosphate receptor (IP_3R1; Sato et al., 2004) and the canonical transient receptor potential-3 (TRPC3; Mio et al., 2005; Mio, Ogura, Kiyonaka, Hiroaki et al., 2007) using single-particle reconstruction. This was achieved by advances in the area of the biochemistry of extremely fragile membrane proteins and originally developed image analysis software. Comparison of these proteins revealed the structural similarities and divergence of the six-TM-type membrane-integral cation channels.

2. Reconstruction from electron microscopic images

2.1. Sample preparation

As the 6-TM-type cation channels were integrated into the plasma membrane, they were solubilized from the membrane fraction by homogenizing in detergent-containing buffer. The extracted channel proteins were purified by conventional biochemical techniques until

they presented a single band in SDS–PAGE. The voltage-sensitive sodium channel was extracted from the electric organ of the electric eel, *Electrophorus electricus electroplax*, in which the sodium channels are concentrated. We tested many detergents and their combinations, and found that Lubrol-PX (polyoxyethylene-9-lauryl ether) was the most effective in solubilizing sodium channel protein from the cell membranes without denaturation (Sato *et al.*, 1998). IP$_3$R1 was solubilized and purified from mouse cerebella (Hamada *et al.*, 2002). They used CHAPS {3-[(3-cholamidopropyl)dimethyl-ammonio]-1-propanesulfonate} in extracting IP$_3$R1 protein from the membrane. These channels were purified from crude protein extract by immunoaffinity chromatography using specific antibodies. To remove further contaminants to the sodium channel, gel filtration chromatography was applied.

Although TRPC3 localizes at a relatively high level in the brain and the central nervous system, it is too scarce for purification and analysis. Therefore, we expressed TRPC3 heterologously in HEK293 cells as FLAG-tag fused proteins and applied a two-step purification process: affinity chromatography and gel filtration chromatography (Mio *et al.*, 2005). Intact channel function of the FLAG-tagged TRPC3 was confirmed by ATP-induced increase in Ca^{2+} intake in transfected cells and by diacylglycerol analogue-induced (1-oleoyl-2-acetyl-*sn*-glycerol; OAG) Mn^{2+} influx (Mio *et al.*, 2005). Formation of proper stoichiometry in the purified protein (*i.e.* tetramer assembly of TRPC3) was confirmed by native–PAGE analysis and chemical cross-linking techniques (Mio *et al.*, 2005). The purity of TRPC3 in the final preparation was estimated to be more than 95% in the SDS–PAGE.

2.2. Electron microscopy

Particle images were recorded using a helium-cooled cryo-electron microscope, which was developed to minimize radiation damage to the specimen (Fujiyoshi, 1998). Purified proteins (0.5–1.0 mg ml^{-1}) were applied to a pre-irradiated holey carbon grid (Miyazawa *et al.*, 1999), which was immediately frozen by plunging it into liquid ethane cooled by liquid nitrogen (Adrian *et al.*, 1984). The grid was transferred into a JEOL JEM3000SFF cryo-electron microscope operating at an acceleration voltage of 300 kV, and kept at 4.2 K. In the noisy raw images, detergent-solubilized sodium channels are observed as slightly higher density particles [indicated by white squares in Fig. 1(*a*)]. The particles are circular or polygonal, depending on orientation. Images were recorded on Kodak SO163 film at a nominal magnification of ×38500 using low-dose procedures (< 20 electrons Å^{-2}) and digitized using a Scitex Leafscan 45 scanner (Leaf Systems Inc.) for statistical analysis.

Particle images are much more clearly observed using the negative staining technique. Solubilized protein of approximately 50–100 µg ml^{-1} was adsorbed by thin carbon film rendered hydrophilic by glow-discharge at low air pressure. The grid surface was washed with drops of 0.1 *M* NH$_4$HCO$_3$ solution and then negatively stained with 0.75% uranyl formate solution. Micrographs of negatively stained particles were recorded with a Hitachi H7000 or H8000 transmission electron microscope at ×80000 magnification with 100 kV acceleration voltages. Negatively stained sodium channels are shown in Fig. 1(*b*) at the same magnification as the cryo-EM images. In the figure, protein is displayed in bright shades. In addition to stain deposition at the periphery of the particles, hydrophilic regions of the molecules are also stained.

EM is also an effective tool when used as a 'quality check' of the specimen at each purification step. EM images of protein molecules provide extensive information about the formation of aggregates, structural deformation and the purity of the target protein (Mio,

Ogura, Kiyonaka, Mori & Sato, 2007). In the reconstruction from the negatively stained EM images, the resolution is somewhat limited by minor protein deformation owing to attachment to the grid surface, dryness and acidic stain solution. However, our results confirm that negatively stained particle images are consistent with cryo-data in molecular shape, dimensions and inner structures.

2.3. Single-particle analysis

We have developed and improved programs for the analysis. In current systems, particle images were automatically picked up by our original programs. Primary selection of the particles from digitized images was performed by the auto-accumulation method using simulated annealing (Ogura & Sato, 2004*b*). The selected particles (200–300 images) were further used to train the three-layer neural network auto-picking system (Ogura & Sato, 2004*a*). Particles touching neighbouring particles were discarded manually.

Image analysis was performed in three major refinement steps. In the first step, particle images were corrected for the contrast transfer function of the electron microscope (Cs = 1.6 mm, acceleration voltage = 300 kV) using the defocus values determined with the Imagic V system (van Heel *et al.*, 1996) and aligned rotationally and translationally (Frank, 2006; van Heel *et al.*, 2000) using the reference free method (Ogura & Sato, 2004*a*). They were then grouped into clusters using the modified Growing Neural Gas classification algorithm (Ogura *et al.*, 2003). The resulting averages were used as new references, and this cycle was repeated until convergence. For the second step, the Euler angles of the class averages were determined by the echo-correlated three-dimensional reconstruction method using simulated annealing (Ogura & Sato, 2006), assuming a fourfold symmetry, and were used to calculate a three-dimensional structure by the SIRT method (Penczek *et al.*, 1992). The reprojections from the initial volume were employed as references for multi-reference alignment. Each image in the library was aligned and clustered, providing improved cluster averages, and a new three-dimensional map was generated by the reconstruction method using simulated annealing without three-dimensional reference and reprojected as above. For the third step, the three-dimensional map was refined by the projection matching method (Penczek *et al.*, 1994).

Images of the sodium channel at each reconstruction step are shown in Fig. 2. The Fourier shell correlation function was used to assess the resolution of the final three-dimensional map (Harauz & van Heel, 1986). Using 11991–135909 particle images, we obtained three-dimensional densities at 15–20 Å resolution.

3. Structural perspective of 6-TM-type cation channels

3.1. Overall structure

Three different types of 6-TM channels were reconstructed from the cryo-EM images (Sato *et al.*, 2001, 2004; Mio, Ogura, Kiyonaka, Hiroaki *et al.*, 2007). The sodium channel has four 6-TM repeats and forms a pseudo-tetramer, whereas IP$_3$R1 and TRPC3 form homo-tetramers (Fig. 3, top right of each section).

These 6-TM-type cation channels have several structural features in common. They all have a bell-shaped structure composed of a relatively small extracellular domain, a protein-dense transmembrane domain, and a larger cytoplasmic domain (Fig. 3, left image of each section). The transmembrane regions of ion channels are distinguished by a seamless belt-like structure at the boundary of the plasma membrane. Despite a large variance in the constituting molecular masses, all these channels have a double-layered structure (Fig. 3, bottom right of each section).

The molecular orientation across the membrane was determined by labeling purified channel proteins with specific antibodies followed by EM observation. In all three channels, the larger ends of the particles are assigned in the cytoplasm. Fig. 2(e) demonstrates the sodium channels decorated with antibodies specific to the channel's cytoplasmic N-terminus.

3.2. Structural divergence of the cytoplasmic domain

A detailed structural analysis of each channel reveals a divergence in the cytoplasmic domain that matches various physiological functions. The voltage-gated sodium channel generates and transmits electric pulses in neurons. In our reconstruction, large vestibules were
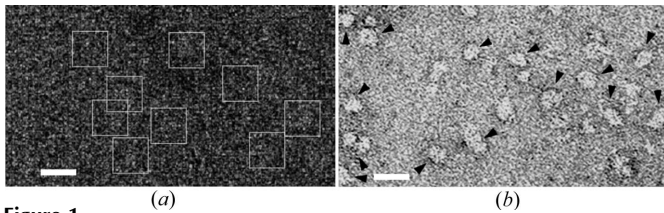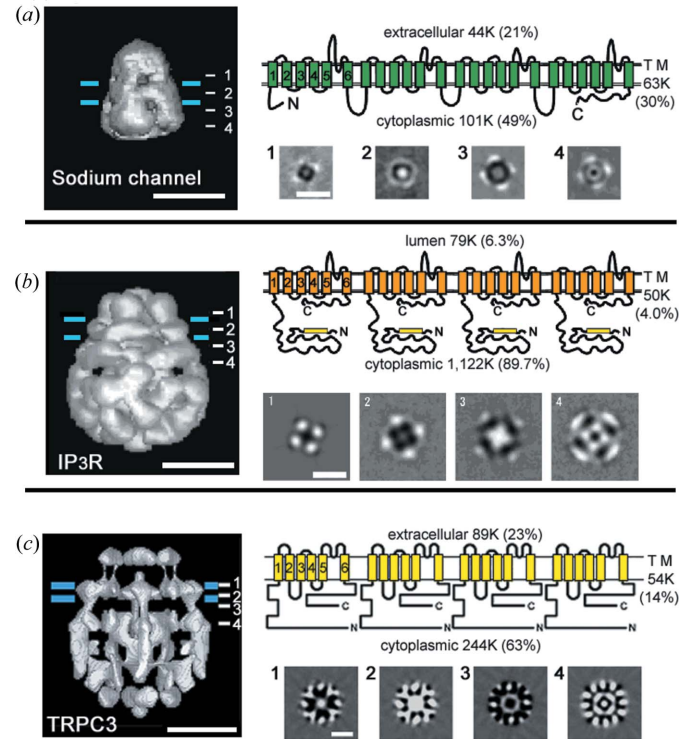

Figure 1
(a) Cryo-EM image of ice-embedded sodium channels extracted from the electric organ of the electric eel, *Electrophorus electricus electroplax*. Channel proteins are marked by white squares. (b) Micrograph of negatively stained sodium channels. As demonstrated by arrowheads, particles are of uniform size but different shapes. This indicates attachment to the grid surface at various angles. The scale bars represent 200 Å.
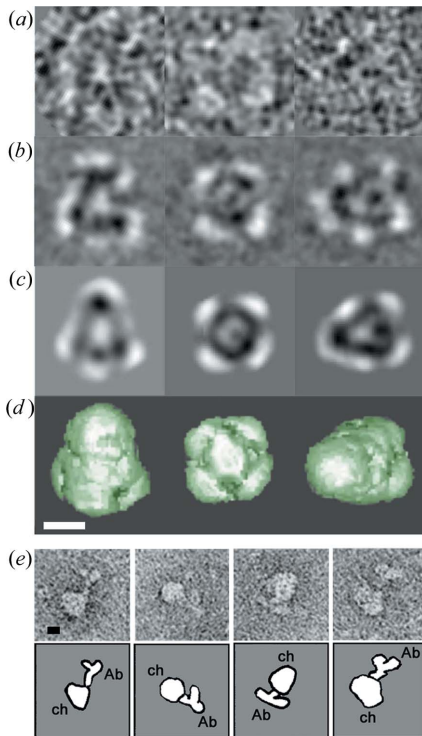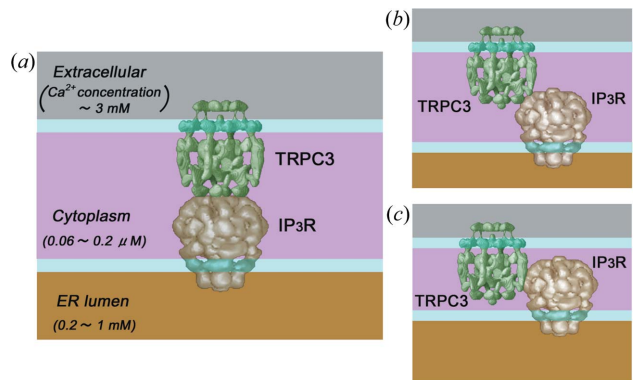

Figure 2
Three-dimensional reconstruction of the voltage-sensitive sodium channel from cryo-EM images. (a) Raw images of the sodium channel with different Euler angles. (b) Corresponding class averages (two-dimensional averages) for each raw image. An improved signal-to-noise ratio revealed characteristic views of the sodium channel. (c) Corresponding projection images from the three-dimensional structure and (d) surface views of the three-dimensional reconstruction. (e) EM of negatively stained sodium channel–antibody complexes. The cytoplasmic region was assigned by the binding of the antibody against the N-terminal sequence of the channel protein. The densities of the channel proteins and antibodies are indicated in the figures by ch and Ab, respectively. The scale bars represent 50 Å.

observed just beneath the membrane (Fig. 3a). This indicates that membrane-permeated Na^+ may immediately shunt to the sides of the channel. This process drastically changes the membrane potential and opens the gates of adjacent sodium channels, which may be part of

Figure 3
Structures of (a) the voltage-sensitive sodium channel, (b) the type-1 IP$_3$ receptor and (c) the TRPC3 channel. Surface-rendered representations of the reconstructed 6-TM cation channels are shown on the left of each part of the figure. The putative transmembrane zone is indicated by two blue lines approximately 30 Å apart. The predicted membrane topologies of these channels are represented with loops and terminal extensions in the top right of each part. Estimated volumes for the extracellular (or luminal), transmembrane and cytoplasmic domains are also indicated. Sections parallel to the membrane plane through the density maps are shown in the bottom right of each part. The positions marked by numbers 1–4 correspond to the numbers on the right-hand side of the surface-rendered representations. The scale bars represent 100 Å.

Figure 4
Three possible binding models between TRPC3 and type-1 IP$_3$ receptor. (a) Top-to-top binding at the center of both channels. The large dimensions of TRPC3 (green) imply a possible top-to-top binding with IP$_3$R1 (brown), although a conformational change is needed for their close contact. The large space between the two membranes enables simultaneous association between TRPC3 and macromolecules including IP$_3$R1 and PLCγ (Kiselyov *et al.*, 1998; Nishida *et al.*, 2003; van Rossum *et al.*, 2005). (b) Corner binding reduces the space between the membranes. (c) Side-by-side binding results in the narrowest membrane distance.

voltage-sensitive signal transduction mechanisms on the surfaces of the nerve cells. In contrast, a large number of pores open over the entire surface of the cytoplasmic domain of the IP$_3$R1 molecule (Fig. 3b). A biphasic Ca^{2+} increase is frequently observed in intracellular Ca^{2+} concentration when cells are stimulated by ligands against cell surface receptors (Bird *et al.*, 1991; Morishita *et al.*, 1989; Takuwa *et al.*, 1987). The initial increase is usually conducted by Ca^{2+} release from internal stores, and the long-lasting delayed increase is by Ca^{2+} intake. The porous balloon structure of IP$_3$R1 seems effective for the rapid Ca^{2+} release from the ER.

The three-dimensional reconstruction of TRPC3 reveals a cavern structure as an inner layer (Fig. 3c). Ions passed through the transmembrane domain enter a large cavern of 60 Å in width and 85 Å in height, with a small spherical density at the center. This cavern seems to be basically a closed space except for four holes at the bottom. The permeated ions may be suspended or diluted there before being released into the cells. Because TRPC3 is a candidate for the store-operated channel (SOC), *i.e.* permeating Ca^{2+} in response to the shortage of internal stores, this cavern structure may suppress the rapid increase of intracellular Ca^{2+} concentration. The cavern structure is unique when compared with the previously reported structure of voltage-sensitive cation channels, which have multiple large side openings for ion release just beneath the membrane (Long *et al.*, 2005; Sato *et al.*, 2001). Another unique aspect of the TRPC3 cytoplasmic domain is its highly expanded wireframe structure (Fig. 3c). Recent studies have established that the TRP family are molecular sensors for a broad range of stimuli, such as tastes, pheromones, temperature, mechanical stretching and intracellular messengers (Montell, 2005; Pedersen *et al.*, 2005; Ramsey *et al.*, 2006). TRPC3's large cytoplasmic domain may provide space for simultaneous coupling with multiple signal molecules. The large dimensions of TRPC3 also allow the possibility of a top-to-top binding with IP$_3$R1 (*i.e.* 1:1 binding; Fig. 4a), in which the four protuberances at the cytoplasmic end of TRPC3 fit well in physical docking with the four grooves of its counterpart IP$_3$R1, although other docking mechanisms such as side-by-side binding are also possible.

4. Future directions

In spite of the limited resolution, reconstruction from EM images has great advantages for understanding the structure of molecules that do not easily crystallize. Recent improvements of particle pick-up systems, including our automated systems, have made the recognition of particles from noisy EM images easier (Nicholson & Glaeser, 2001). Template-matching cross-correlation methods have been mainly used to select very large proteins or viruses, since they require reliable templates of projections (Frank & Wagenknecht, 1984; Roseman, 2003; Thuman-Commike & Chiu, 1996). We have recently determined the three-dimensional structure of a small novel cation channel (the TRIC channel; 99 kDa for trimer) from a negatively stained specimen (Yazawa *et al.*, 2007). Further improvement of software will allow us to analyze even smaller molecules.

Another important goal for single-particle analysis is to improve resolution. Improvement of purification protocols, such as the finding of more suitable buffers or of stabilizing ligands, will help to improve the resolution. Accumulation of a large number of projection images, which will be achieved by the automated particle pick-up systems, will also be necessary. The structures of the functional complexes (ion channels with regulator proteins) should also be clarified in future.

References

Adrian, M., Dubochet, J., Lepault, J. & McDowall, A. W. (1984). *Nature* (*London*), **308**, 32–36.
Bird, G. S., Rossier, M. F., Hughes, A. R., Shears, S. B., Armstrong, D. L. & Putney, J. W. Jr (1991). *Nature* (*London*), **352**, 162–165.
Frank, J. (2006). *Three-Dimensional Electron Microscopy of Macromolecular Assemblies: Visualization of Biological Molecules in Their Native State*. New York: Oxford University Press.
Frank, J. & Wagenknecht, T. (1984). *Ultramicroscopy*, **12**, 169–175.
Fujiyoshi, Y. (1998). *Adv. Biophys.* **35**, 25–80.
Hamada, K., Miyata, T., Mayanagi, K., Hirota, J. & Mikoshiba, K. (2002). *J. Biol. Chem.* **277**, 21115–21118.
Harauz, G. & van Heel, M. (1986). *Optik*, **73**, 146–156.
Heel, M. van, Gowen, B., Matadeen, R., Orlova, E. V., Finn, R., Pape, T., Cohen, D., Stark, H., Schmidt, R., Schatz, M. & Patwardhan, A. (2000). *Q. Rev. Biophys.* **33**, 307–369.
Heel, M. van, Harauz, G., Orlova, E. V., Schmidt, R. & Schatz, M. (1996). *J. Struct. Biol.* **116**, 17–24.
Henderson, R. (2004). *Q. Rev. Biophys.* **37**, 3–13.
Hille, B. (2001). *Ion Channels of Excitable Membranes*, 3rd ed. Sunderland: Sinauer.
Kiselyov, K., Xu, X., Mozhayeva, G., Kuo, T., Pessah, I., Mignery, G., Zhu, X., Birnbaumer, L. & Muallem, S. (1998). *Nature* (*London*), **396**, 478–482.
Long, S. B., Campbell, E. B. & Mackinnon, R. (2005). *Science*, **309**, 897–903.
Mio, K., Ogura, T., Hara, Y., Mori, Y. & Sato, C. (2005). *Biochem. Biophys. Res. Commun.* **333**, 768–777.
Mio, K., Ogura, T., Kiyonaka, S., Hiroaki, Y., Tanimura, Y., Fujiyoshi, Y., Mori, Y. & Sato, C. (2007). *J. Mol. Biol.* **367**, 373–383.
Mio, K., Ogura, T., Kiyonaka, S., Mori, Y. & Sato, C. (2007). *J. Electron Microsc.* **56**, 111–117.
Miyazawa, A., Fujiyoshi, Y., Stowell, M. & Unwin, N. (1999). *J. Mol. Biol.* **288**, 765–786.
Montell, C. (2005). *Sci. STKE*, **2005**, re3.
Morishita, R., Higaki, J. & Ogihara, T. (1989). *Biochem. Biophys. Res. Commun.* **160**, 628–632.
Nicholson, W. V. & Glaeser, R. M. (2001). *J. Struct. Biol.* **133**, 90–101.
Nishida, M., Sugimoto, K., Hara, Y., Mori, E., Morii, T., Kurosaki, T. & Mori, Y. (2003). *EMBO J.* **22**, 4677–4688.
Ogura, T., Iwasaki, K. & Sato, C. (2003). *J. Struct. Biol.* **143**, 185–200.
Ogura, T. & Sato, C. (2004a). *J. Struct. Biol.* **145**, 63–75.
Ogura, T. & Sato, C. (2004b). *J. Struct. Biol.* **146**, 344–358.
Ogura, T. & Sato, C. (2006). *J. Struct. Biol.* **156**, 371–386.
Pedersen, S. F., Owsianik, G. & Nilius, B. (2005). *Cell Calcium*, **38**, 233–252.
Penczek, P. A., Grassucci, R. A. & Frank, J. (1994). *Ultramicroscopy*, **53**, 251–270.
Penczek, P., Radermacher, M. & Frank, J. (1992). *Ultramicroscopy*, **40**, 33–53.
Ramsey, I. S., Delling, M. & Clapham, D. E. (2006). *Annu. Rev. Physiol.* **68**, 619–647.
Roseman, A. M. (2003). *Ultramicroscopy*, **94**, 225–236.
Rossum, D. B. van, Patterson, R. L., Sharma, S., Barrow, R. K., Kornberg, M., Gill, D. L. & Snyder, S. H. (2005). *Nature* (*London*), **434**, 99–104.
Sato, C., Hamada, K., Ogura, T., Miyazawa, A., Iwasaki, K., Hiroaki, Y., Tani, K., Terauchi, A., Fujiyoshi, Y. & Mikoshiba, K. (2004). *J. Mol. Biol.* **336**, 155–164.
Sato, C., Sato, M., Iwasaki, A., Doi, T. & Engel, A. (1998). *J. Struct. Biol.* **121**, 314–325.
Sato, C., Ueno, Y., Asai, K., Takahashi, K., Sato, M., Engel, A. & Fujiyoshi, Y. (2001). *Nature* (*London*), **409**, 1047–1051.
Takuwa, Y., Takuwa, N. & Rasmussen, H. (1987). *Am. J. Physiol.* **253**, C817–827.
Thuman-Commike, P. A. & Chiu, W. (1996). *J. Struct. Biol.* **116**, 41–47.
Yazawa, M. *et al.* (2007). *Nature* (*London*), **448**, 78–82.